# Recent highlights from the Belle and Belle II experiments⋆

Yubo Han, On behalf of the Belle and Belle II Collaborations[a,*,1]

[a]DESY, Notkestraße 85, Hamburg, 22607, Germany

ARTICLE INFO

*Keywords*:
$e^+e^-$ Experiments
Lepton flavor universality tests
CKM physics
Rare $B$ decays
Spectroscopy
Inputs to the $g_\mu - 2$

ABSTRACT

The Belle experiment at the KEKB collider in Tsukuba operated as a B-factory until 2018, making significant contributions to flavor physics. Building on this legacy, the Belle II experiment, an upgraded version, now operates at the SuperKEKB energy-asymmetric $e^+e^-$ collider. Belle II has collected 424 fb$^{-1}$ of data, including 363 fb$^{-1}$ at the $\Upsilon(4S)$ resonance. A wide range of physics topics can be studies with this data. In this proceeding, we review our latest results, which include tests of lepton flavor universality, Cabibbo-Kobayashi-Maskawa physics, searches for rare $B$-meson decays, and spectroscopy studies. We also discuss contributions to the $g_\mu - 2$ prediction.

## 1. Introduction

The Belle II experiment [1, 2] is conducted at the SuperKEKB accelerator located in Tsukuba, Japan. SuperKEKB, an upgraded version of the KEKB collider, operates at the energy corresponding to the $\Upsilon(4S)$ resonance, allowing for the production of many $B\bar{B}$ pairs at threshold.

It utilises asymmetric beam energies, with electrons accelerated to 7 GeV and positrons to 4 GeV. These asymmetric beam energies provides a boost to the centre-of-mass frame. SuperKEKB was designed to achieve a target luminosity 30 times greater than that of its predecessor, KEKB, by employing higher beam currents and advanced nano-beam technology. To date, it had achieved a instantaneous luminosity of $4.7 \times 10^{34}\,\mathrm{cm}^{-2}\,\mathrm{s}^{-1}$, which is a new world record.

The Belle II detector, optimised for high-luminosity, is composed of multiple sub-detectors arranged around the beam pipe. At the inner most region is a silicon vertex detector, consisting of a pixel and double-sided silicon strip detector, essential for precise vertex reconstruction. This is followed by a central drift chamber (CDC) that measures the momenta and charge of particles. Particle identification (PID) is achieved through a time-of-propagation (TOP) counter in the barrel region and an aerogel ring-imaging Cherenkov (ARICH) detector in the forward endcap. These systems allow for effective discrimination between particle types, such as pions and kaons, crucial for flavor tagging. The electromagnetic calorimeter (ECL), responsible for reconstructing photons and differentiating electrons, operates within a 1.5 T magnetic field generated by a superconducting solenoid. Additionally, a dedicated system for identifying $K_L^0$ and muons is embedded in the solenoid's flux return.

Belle II provides several scientific advantages. Its well-defined initial state in electron-positron collisions offers a clean environment for precise measurements. The quantum-coherent $B$-meson pairs at the $\Upsilon(4S)$ resonance significantly enhances our flavor tagging capability. The boosted center-of-mass system enables time-dependent measurements, while the nearly hermetic detector structure, with excellent particle identification, allows the study of decays involving neutral particles or invisible states like neutrinos. Furthermore, Belle II's ability to operate at various center-of-mass energies supports a wide range of physics studies beyond just $B$-mesons.

After beginning data collection in 2019, Belle II accumulated 424 fb$^{-1}$ of data during Run 1, with 363 fb$^{-1}$ collected with at $\Upsilon(4S)$ resonance. Following a long shutdown (LS1) for upgrades, including the installation of a two-layer pixel detector (PXD), beam pipe replacement, and improvements to the TOP and CDC systems, data taking was resumed in early 2024. Since then, Belle II has collected over 100 fb$^{-1}$ of data with approximately 90% efficiency. However, challenges with beam losses resulting in high radiation exposure in the interaction region led to the precautionary shutdown of the PXD. Despite this, Belle II is operating stably at a luminosity of $4.5 \times 10^{34}\,\mathrm{cm}^{-2}\,\mathrm{s}^{-1}$.

In this proceeding, we highlight selected recent results from both the Belle and Belle II experiments, including tests of lepton flavor universality, studies on CKM physics, searches for rare $B$-meson decays, spectroscopy studies, and contributes to the $g_\mu - 2$ prediction.

## 2. Lepton-flavor universality tests

In the standard model (SM), electroweak gauge bosons couple equally to the three lepton generations $(e, \mu, \tau)$, a symmetry known as lepton universality (LU). Semileptonic $B$-meson decays, $B$ decays to a charmed hadronic state, a lepton, and a neutrino, provide excellent sensitivities for testing the LU. One key observable in such studies is the branching fraction ratio

$$R(H_{\tau/l}) = \frac{\mathcal{B}(B \to H\tau\nu_\tau)}{\mathcal{B}(B \to Hl\nu_l)},$$

where $l$ is either an $e$ or a $\mu$ and $H$ is an hadron, is a sensitive probe for the universality of the third generation.

⋆

*Corresponding author
yubo.han@desy.de (Y.H.O.b.o.t.B.a.B.I. Collaborations)
(Y.H.O.b.o.t.B.a.B.I. Collaborations)
ORCID(s):
1

The final state hadron $H$ can be $D^{(*)}$, $\pi$, or other hadrons from exclusive modes. It could also be an inclusive hadronic system $X$. This ratio provides a significant advantage as it partially cancels out both theoretical uncertainties and common experimental systematic uncertainties, the sensitivity is enhanced because of that.

Such tests of LU has been done on different experiments (BABAR [3, 4], Belle [5], Belle II [6] and LHCb [7]). The combination of the results has a $3.3\sigma$ tension with the standard model expectation, which could indicate an enhanced coupling of the $b$ quark to the $\tau$ lepton.

In the following sections, we present an inclusive test of $R(X_{\tau/l})$ and an examination of light-lepton university in $\tau$ decays utilizing data collected by Belle II.

## 2.1. Inclusive Test of the $b \to c\tau\nu$ Anomaly

We present a complementary probe of LU through the first measurement of the tau-to-light-lepton ratio of inclusive semileptonic B-meson branching fractions:

$$R(X_{\tau/l}) \equiv \frac{\mathcal{B}(B \to X\tau\nu)}{\mathcal{B}(B \to Xl\nu)},$$

which is statistically and theoretically distinct from the $R(D^{(*)})$ measurement [8].

For this analysis, we utilize the dataset collected by the Belle II experiment between 2019 and 2021 at a center-of-mass energy of $\sqrt{s} = 10.58$ GeV, corresponding to an integrated luminosity of 189 fb$^{-1}$. And additional off-resonance dataset (18 fb$^{-1}$) collected with 60 MeV below the $\Upsilon(4S)$ is used to study the background from continuum process $e^+e^- \to q\bar{q}$.

The Full Event Interpretation [9] was applied to reconstruct a $B$-meson candidate in a fully hadronic decay mode, which is referred to as a $B_{\text{tag}}$. From the remaining part of events, we select a single-lepton candidate, and the hadronic $X$ is reconstructed from any remaining tracks and energy deposits in the ECL that are not associated with identified tracks.

The signal and normalization yields for the electron and muon modes are extracted simultaneously with a maximum-likelihood fit to the binned two-dimensional distribution of $p_l^B$ and $M^2_{\text{missing}}$. The largest uncertainties are associated with the experimental and simulation sample sizes. After all the corrections and selections, we determined the efficiencies for the electron mode and the muon mode. The signal yields are extracted by fitting the experimental $(p_l^B, M^2_{\text{missing}})$ spectra as shown in Fig. 1. The statistic and systematic uncertainties are incorporated in the fit via nuisance parameters, one for each $(p_l^B, M^2_{\text{missing}})$ bin for each component.

The branching-fraction uncertainties are considered for the fit. Tagging efficiency cancels in the $R(X_{\tau/l})$ ratio which is supported by the agreement between experimental and simulated distribution of the relevant $B$ quantities. The $R(X_\tau/l)$ for electrons and muons are

$$R(X_{\tau/e}) = 0.232 \pm 0.020(\text{stat}) \pm 0.037(\text{syst}),$$

$$R(X_{\tau/\mu}) = 0.222 \pm 0.027(\text{stat}) \pm 0.050(\text{syst}),$$

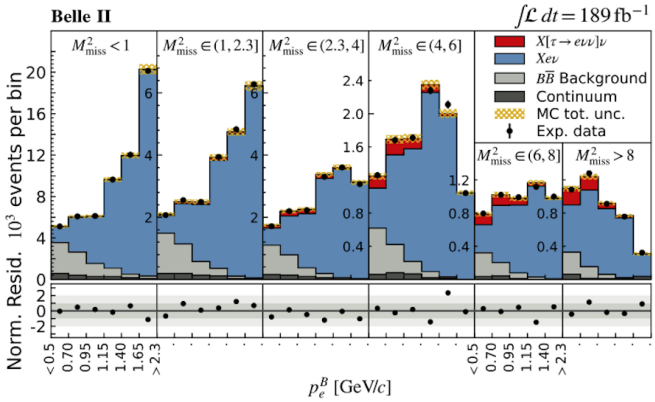


**Figure 1:** Two-dimensional distributions of electron momentum in the $B_{sig}$ rest frame $p_l^B$ and the missing mass squared $M^2_{\text{missing}}$, flattened to one dimension in intervals as used in the signal extraction fit, with the fit results overlaid.

respectively. The combined result is

$$R(X_\tau/l) = 0.228 \pm 0.016(\text{stat}) \pm 0.036(\text{syst}),$$

The observed result is in agreement with the SM predictions. After removing the expected contributions from $B \to D^{**}_{(\text{gap})}\tau(l)\nu$ and $B \to X_u\tau(l)\nu$ from the measured $R(X)$, the remaining component provides a distinct cross-check of the exclusive $R(D^{(*)})$. As shown in Fig. 2, the result aligns with the world averaged $R(D^{(*)})$ and also the SM predictions within the current uncertainties [10]. More details on this measurement can be found in [11].

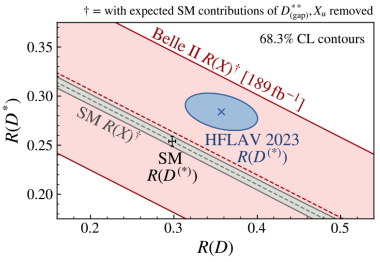


**Figure 2:** $R(D^{(*)})$ from the measured $R(X)$ value (red), compared to the world average and the SM prediction.

## 2.2. Light-lepton Universality in $\tau$ Decays

LU tests can be done between the light-leptons. The tests in $\tau$ decays are sensitive not only to charged currents but also to non-SM contributions of weak neutral currents. The tests rely on measurements of $\tau$ properties like mass, lifetime and branching fractions of $\tau$ decays to lighter leptons of hadrons. The $e - \mu$ universality is tested by comparing the measured rates of leptonic $\tau$-decays:

$$R_\mu = \frac{\mathcal{B}(\tau^- \to \mu^-\bar{\nu}_\mu\nu_\tau)}{\mathcal{B}(\tau^- \to e^-\bar{\nu}_e\nu_\tau)},$$

This allows us to constrain the ratio of the effective coupling strengths, $g_e$ and $g_\mu$ to the $W^\pm$. The ratio is given by

$$|\frac{g_\mu}{g_e}| = \sqrt{R_\mu \frac{f(m_e^2/m_\tau^2)}{f(m_\mu^2/m_\tau^2)}},$$

The challenge of this measurement lies in the precise determination the ratio of branching fractions $R_\mu$. Previous tests have been performed by the CLEO [12] and BaBar [13] collaborations. The most precise determination to date is from BaBar: $R_\mu = 0.9796 \pm 0.0016(\text{stat}) \pm 0.0036(\text{syst})$. The leading systematic source comes from the lepton identification, which propagates to 0.2% precision on the ratio of coupling strengths. The current world average value $|g_\mu/g_e|_\tau = 1.0019 \pm 0.0014$ [10] is consistent with the SM prediction ($R_\mu^{\text{SM}} = 0.9726$).

We report a measurement of $R_\mu$ with Belle II data collected between 2019 and 2022 with centre-of-mass energy of 10.58 GeV, corresponding to an integrated luminosity of $362 \pm 2\ \text{fb}^{-1}$ which translates to about $333 \times 10^6\ e^+e^- \to \tau^+\tau^-$ events. The $R_\mu$ is determined from events in which $\tau$ decays either to $\tau^- \to e^-\bar{\nu}_e\nu_\tau$ or $\tau^- \to \mu^-\bar{\nu}_\mu\nu_\tau$, the other $\tau$ decays hadronically.

The selections are optimzied and applied to both modes, a binned maximum likelihood fit is performed on momentum spectra to extract the signal candidates. Distribution of the muon and electron candidate momentum with fit result overlaid is shown in Fig. 3.

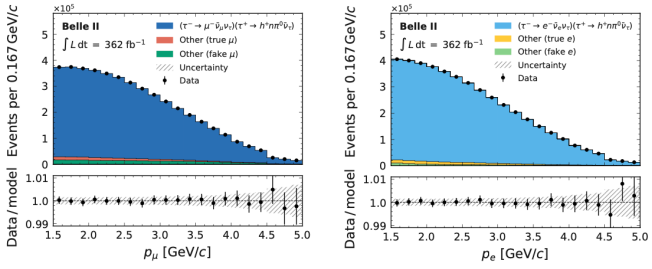


**Figure 3:** Observed momentum distribution for $\tau^- \to \mu^-\bar{\nu}_\mu\nu_\tau$ (left) and $\tau^- \to e^-\bar{\nu}_e\nu_\tau$ (right) candidates with fit results overlaid. The lower panel shows the ratio between data and fit results. The hatched area indicates the possible variation of the fitted yields due to systematic effects, with the constraints of the nuisance parameters reduced to their fit uncertainties and correlations taken into account.

All systematic effects are modelled directly in the likelihood function. The ratio of branching fractions are measured to be

$$R_\mu = \frac{\mathcal{B}(\tau^- \to \mu^-\bar{\nu}_\mu\nu_\tau)}{\mathcal{B}(\tau^- \to e^-\bar{\nu}_e\nu_\tau)} = 0.9675 \pm 0.0007 \pm 0.0036,$$

The result is consistent with previous measurements and is the most precise measurement from a single experiment to date and consistent with the SM prediction. The comparison of the results from this study with these from other experiments are shown in Fig. 4.

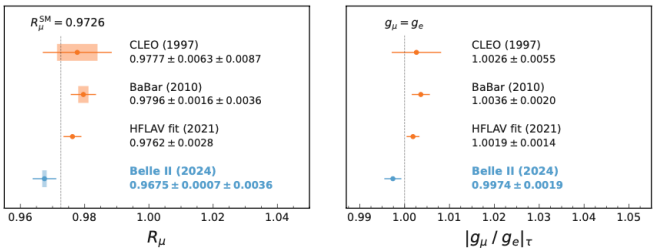


**Figure 4:** Determinations of $R_\mu$ (left) and $|g_\mu/g_e|_\tau$ (right) from previous individual measurements and the fit from the Heavy Flavor Averaging Group, compared with the result of this work. The shaded areas represent the statistical uncertainties, while the error bars indicate the total uncertainties. The vertical dashed line indicates the SM prediction, including mass effects.

## 3. CKM physics

The Cabibbo-Kobayashi-Maskawa (CKM) matrix in the SM describes the quark mixing and accounts for CP-violation in the quark sector [14, 15]. One of the crucial tests of the SM is to measure the magnitudes of the CKM matrix elements as precisely as possible. These measurements are crucial for validating the SM and exploring potential new physics beyond it. The $V_{xb}$, where $x$ represents either the $u$ or $c$ quark, can be determined by measuring the branching fraction of $B \to X_x l\nu_l$ decays, which is proportional to $|V_{xb}|^2$. $|V_{xb}|$ can be determined by inclusive method, no specific final state is reconstructed, and exclusive method which reconstruct a specific final state. These two methods have complementary uncertainties introduced by their theoretical descriptions.

Several measurements have been conducted by both the Belle and Belle II experiments [16, 17, 18]. The world averages of $|V_{xb}|$ from experimental data obtained by exclusive and inclusive determinations exhibits a disagreement of approximately 3 standard deviations [10]. We carried out several measurements using new strategies to further investigate these tensions.

### 3.1. Exclusive $|V_{ub}|$ from simultaneous measurements of $B^0 \to \pi^- l^+ \nu_l$, $B^+ \to \rho^0 l^+ \nu_l$

The most experimentally and theoretically reliable exclusive measurements of $|V_{ub}|$ come from $B \to \pi l \nu_l$ decays. The most precise value of $|V_{ub}|$ is from this mode. A simultaneous measurement of $B^0 \to \pi^- l^+ \nu_l$ with $B \to \rho l \nu_l$ allows for an additional measurement while accounting for decays of one type that are reconstructed as the other. Therefore, we performed this measurement to simultaneously reconstruct $B^0 \to \pi^- l^+ \nu_l$ with $B^+ \to \rho^0 l^+ \nu_l$ (charge conjugation implied throughout).

This measurement explores a data sample of 364 $\text{fb}^{-1}$, which corresponding to 387 million $B\bar{B}$ meson pairs recorded by the Belle II detector between 2019 and 2022. The two signal decays are reconstructed without identifying the partner $B$ mesons. The reconstructed events are separated into 13 intervals for the pion mode and 10 intervals for the rho mode of squared momentum transfer $q^2$. The signal yields

of the two modes are simultaneously extracted from a two-dimensional grid of the energy difference $\Delta E = E^*_B - E^*_{\text{beam}}$ and the beam-constrained mass $M_{\text{bc}} = \sqrt{E^{*2}_{\text{beam}} - |p^*_B|^2}$ in each $q^2$ bin as shown in Fig. 5, here $E^*_{\text{beam}}$, $E^*_B$and $P^*_B$ represent the beam energy, reconstructed $B$-meson energy, and reconstructed $B$-meson momentum, respectively, all determined in the center-of-mass (c.m.). With this novel method, cross-feed signals can be properly linked between the two decay modes.

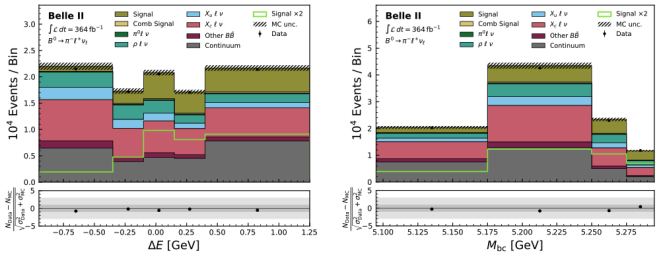


**Figure 5:** Distributions of $\Delta E$ (left) and $M_{\text{bc}}$ (right) reconstructed in Belle II data integrated over the $q^2$ bins for $B^0 \to \pi^- l^+ \nu$ with expected distributions from simulation overlaid. The simulated samples are weighted according to luminosity. The hatched areas include statistical and systematic uncertainties on the simulated distributions. The expected signal distributions (scaled by a factor two) are also shown. The panels below the histograms show the difference between collision and simulated data divided by the combined uncertainty.

The differential branching fractions of $B^0 \to \pi^- l^+ \nu_l$, $B^+ \to \rho^0 l^+ \nu_l$ decays as functions of $q^2$ were measured simultaneously. The partial branching fractions are extracted from the fitted signal yields after efficiency corrections as a function of $q^2$. Furthermore, the total branching fraction is calculated as the sum of these partial branching fractions, with systematic correlations taken into account. As preliminary results, we obtain the total branching fraction:

$$\mathcal{B}(B^0 \to \pi^- l^+ \nu_l) = (1.516 \pm 0.042_{\text{stat}} \pm 0.059_{\text{syst}}) \times 10^{-4},$$

$$\mathcal{B}(B^+ \to \rho^0 l^+ \nu_l) = (1.625 \pm 0.079_{\text{stat}} \pm 0.180_{\text{syst}}) \times 10^{-4},$$

The results are consistent with the world averages and the precision is compatible with respect to previous measurements from Belle and BaBar.

The value of $|V_{ub}|$ is extracted by fitting the measured partial branching fractions as a function of $q^2$, incorporating constraints on non-perturbative hadronic contributions from lattice QCD calculations and light-cone sum rules, or a combination of both as shown in Fig. 6. The values are

$$|V_{ub}|_{B^0 \to \pi^- l^+ \nu_l} = (3.73 \pm 0.07 \pm 0.07 \pm 0.16) \times 10^{-3},$$

$$|V_{ub}|_{B^+ \to \rho^0 l^+ \nu_l} = (3.19 \pm 0.12 \pm 0.17 \pm 0.26) \times 10^{-3},$$

where the uncertainties are statistical, systematic, and theoretical, respectively. The precision is limited by theoretical uncertainties for both cases.

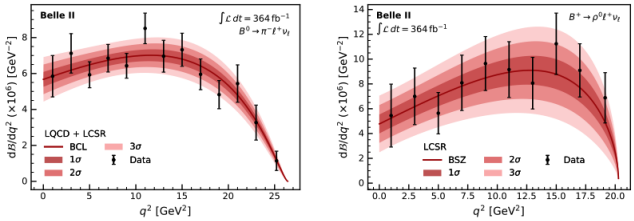


**Figure 6:** Measured partial branching fractions as a function of $q^2$ for $B^0 \to \pi^- l^+ \nu_l$, $B^+ \to \rho^0 l^+ \nu_l$. The fitted differential rates are shown together with the one, two, and three standard-deviation uncertainty bands for fits using constraints on the form factors from LQCD+LCSR and LCSR

## 3.2. $B^0 \to \pi^0\pi^0$ at Belle II

The decay of the neutral bottom-meson into a pair of neutral pions, $B^0 \to \pi^0\pi^0$, plays an important role in the study of the weak interactions of quarks. It helps constrain beyond-SM processes, test and refine hadronic decay models, and provides essential inputs for the determination of the least-well-known angle of the CKM unitarity triangle, $\phi_2$, a fundamental parameter in flavor-changing weak interactions of quarks.

Improved measurements of $\phi_2$ increase the power of tests of CKM-matrix unitarity to provide more stringent bounds on possible SM extensions. Given the presence of contributions from both $b \to u$ ($W$ emission, or tree) and $b \to d$ ($W$ exchange, or penguin) transitions in the decay amplitude, the determination of $\phi_2$ requires measurements of the branching fractions and $CP$ asymmetries of the full set of isospin-related $B \to \pi\pi$ decay modes, i.e., $B^0 \to \pi^+\pi^-$, $B^0 \to \pi^0\pi^0$ and $B^+ \to \pi^+\pi^0$ [19, 20]. Studies of time-dependent $CP$-violating asymmetries involving the $b \to u$ transition is also relevant with $B^0 \to \pi^0\pi^0$ decays. These asymmetries currently offer the most precise way to measure the $\phi_2$, strengthening tests of CKM-matrix unitarity. Currently, the uncertainty in $\phi_2$ is dominated by the uncertainties on the $B^0 \to \pi^0\pi^0$ branching fraction and $CP$-violating flavor-dependent decay-rate asymmetry,

$$\mathcal{A}_{CP}(B^0 \to \pi^0\pi^0) = \frac{\Gamma(\bar{B}^0 \to \pi^0\pi^0) - \Gamma(B^0 \to \pi^0\pi^0)}{\Gamma(\bar{B}^0 \to \pi^0\pi^0) + \Gamma(B^0 \to \pi^0\pi^0)},$$

where $\Gamma$ is the decay width, there are several measurements been done so far. The world-average values $\mathcal{B}(B^0 \to \pi^0\pi^0) = (1.59 \pm 0.26) \times 10^{-6}$ and $\mathcal{A}_{CP}(B^0 \to \pi^0\pi^0) = 0.33 \pm 0.22$ combine measurements reported by the BaBar [21, 22] and Belle [23] collaborations.

We present a measurement of the branching fraction and $CP$ asymmetry for the $B^0 \to \pi^0\pi^0$ decay using a 362 fb$^{-1}$ sample of the data collected by Belle II at energy near threshold at the $\Upsilon(4S)$ resonance and 42.3 fb$^{-1}$ sample collected at a lower energy for background modeling. Such decay is experimentally challenging given that only four photons in the final state are are expected. The reconstruction of photons is based solely on calorimeter information and

therefore has much less precise than the reconstruction of charged particles.

This work supersedes a previous Belle II result [24] that was based on approximately half of the data sample and introduces several significant improvements. We enhance background suppression by increasing the discriminating power of classifiers and simplify the sample composition fit by including the predicted signal flavor obtained through new, more effective algorithms [25]. Additionally, we incorporate a larger fraction of background-only control data into the fit to directly constrain background models from the data, thereby reducing systematic uncertainties. These enhancements lead to a reduction in fractional statistical (systematic) uncertainty by 10% (50%) for the branching fraction, and an absolute uncertainty reduction of 3% (2%) for the $CP$ asymmetry at a given sample size.

The results are extracted with a simultaneous fit to $M_{\rm bc}$, $\Delta E$, C and w where C is the output of a BDT to suppress the continuum background and w is the wrong tag probability. Fig. 7 and Fig. 8 show the signal-enhanced data distributions with fit projections overlaid.

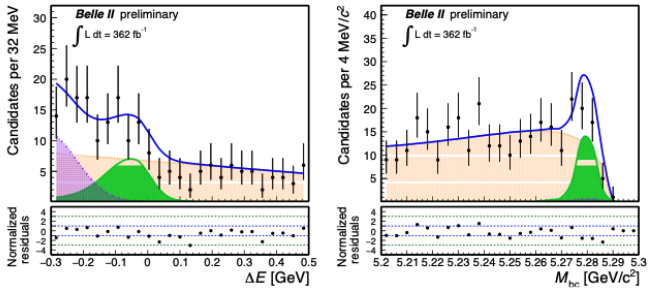


**Figure 7:** Distributions of $\Delta E$ (left) and $M_{\rm bc}$ (right) for the $B^0 \to \pi^0\pi^0$ candidates with positive q tags. The result of the fit to the data is overlaid.

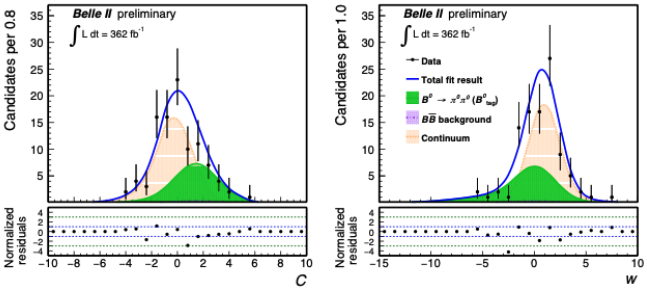


**Figure 8:** Distributions of C (left) and w (right) for the $B^0 \to \pi^0\pi^0$ candidates with positive q tags. The result of the fit to the data is overlaid.

The preliminary results are $\mathcal{B}(B^0 \to \pi^0\pi^0) = (1.26 \pm 0.20 \pm 0.12) \times 10^{-6}$ and $\mathcal{A}_{CP}(B^0 \to \pi^0\pi^0) = 0.06 \pm 0.30 \pm 0.05$, where the first contributions to the uncertainties are statistical and the second systematic. These measurements achieve a precision that is either superior to or comparable with the precision of previous best results, despite being based on smaller datasets.

## 4. Rare B decays

Flavour-Changing Neutral Current (FCNC) transitions in $B$ mesons are rare decays, with branching fractions typically at or below $10^{-5}$. These transitions are forbidden at the tree level and occur via electroweak-loop diagrams, with further suppression arising from CKM matrix elements. Since the SM contributions to these processes are very small, FCNC decays are highly sensitive to potential beyond-Standard Model (BSM) physics.

### 4.1. $B^0 \to \gamma\gamma$ at Belle and Belle II

The double radiative decay $B^0 \to \gamma\gamma$ is a $b \to d$ FCNC transition in the SM. This decay proceeds via electroweak loop diagrams, with the dominant contributions coming from box and penguin diagrams. While a long-distance penguin contribution is theoretically possible, it is expected to be negligible in comparison. There are several measurements been done the most stringent upper limit on the branching fraction is set by BaBar [26] at 90% confidence level with $\mathcal{B}(B^0 \to \gamma\gamma) < 3.2 \times 10^{-7}$.

This decay was previously measured using a fraction of the Belle dataset (104 $\mathrm{fb}^{-1}$). Here, we present a search for the $B^0 \to \gamma\gamma$ decay with improved statistics, utilizing a combined dataset from Belle (694 $\mathrm{fb}^{-1}$) and Belle II (362 $\mathrm{fb}^{-1}$), both collected at the $\Upsilon(4S)$ resonance.

This process is particularly challenging to study due to only two photons in the final state, which leads to significant background contamination. Signal decays are characterized by two nearly back-to-back highly energetic photons in the $e^+e^-$ center-of-mass (c.m.) frame, as $B^0$ mesons are produced almost at rest. A series of requirements on photon candidates are applied to reject the background photons, a BDT is also used to distinguish between photon and $K_L^0$ showers. A requirement on the ECL cluster hit time is also applied to reject the out-of-time QED process. The $B^0 \to \gamma\gamma$ signal candidates are reconstructed by combining two photon candidates and selected using the beam-constrained mass $M_{\rm bc}$ and energy difference $\Delta E$. Another BDT is implemented for $\pi^0/\eta$ veto, we also explore a dedicated BDT for comtinuum suppression.

The signal is extracted using a three-dimensional unbinned maximum likelihood fit to $M_{\rm bc}$, $\Delta E$ and $C'_{\rm BDT}$, where $C'_{\rm BDT}$ is the output of the BDT (the classifier for continuum background suppression mentioned above) transformed using the probability integral transformation. An extended unbinned maximum likelihood fit was performed to the $M_{\rm bc}$, $\Delta E$ and $C'_{\rm BDT}$ distributions simultaneously in Belle and Belle II datasets, which is shown in Fig. 9.

The branching fraction combined is determined to be $(3.7^{+2.2}_{-1.8} \pm 0.5) \times 10^{-8}$ with a total signal (background) yield of $11.0^{+6.5}_{-5.5}$ $(931 \pm 31)$ events. With this result, we set an upper limit of $6.4 \times 10^{-8}$ at 90% confidence level. This result represents a significant improvement over the previous searches by the Babar and Belle collaborations, more details can be found in [27].

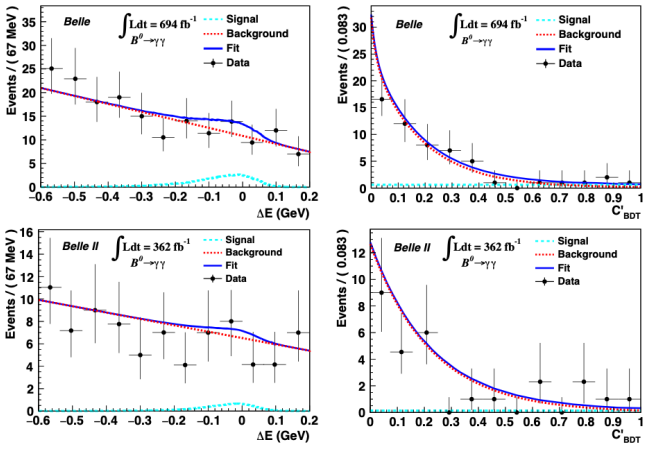


**Figure 9:** Signal enhanced projections of $\Delta E$ and $C'_{\mathrm{BDT}}$ for the $B^0 \to \gamma\gamma$ analysis using the Belle (top) and Belle II (bottom) dataset.

## 4.2. Evidence for $B^+ \to K^+\nu\bar{\nu}$ decays

$B^+ \to K^+\nu\bar{\nu}$ is a FCNC $b \to s\nu\bar{\nu}$ transition, which is highly suppressed in the SM. The rate of this process is very precisely predicted: $\mathcal{B}(B^+ \to K^+\nu\bar{\nu})_{\mathrm{SM}} = (5.6 \pm 0.4) \times 10^{-6}$ [28], with leading theoretical uncertainty arising from hadronic form factors.

This decay is particularly challenging to study due to its rarity and its nature as a three-body decay, with only a single charged track present in the final state. These factors complicate both the detection and analysis, making the study of this process suitable for Belle (II). This decay channel is one of the cleanest within the SM and is highly sensitive to non-SM contributions. To date (before this result), no direct observation of this decay has been made, with previous results providing only upper limits [29, 30, 31]. Belle II offers distinct advantages for studying this decay, including constraints from known initial state kinematics and a lower average multiplicity at the $\Upsilon(4S)$ compared to hadronic collisions, enhancing the ability to isolate and analyze the decay events.

We used a 362 $\mathrm{fb}^{-1}$ Belle II dataset to exploit the inclusive properties of the accompanying $B$-meson in $\Upsilon(4S)$ events to suppress background from other decays of the signal $B$-candidate and light-quark pair production. This method, which leverages the inclusive properties of the $B$-meson produced alongside the signal $B$-meson, is referred to as the Inclusive Tagging Analysis (ITA). To validate the measurement, we performed an auxiliary analysis based on the conventional hadronic reconstruction of the accompanying $B$-meson, referred to as Hadronic Tagging Analysis (HTA). The HTA delivers tighter background control but lower signal reconstruction efficiency, which is in complementary to ITA.

For background suppression, we exploit distinct signal features using machine learning methods trained with simulated data. The signal-reconstruction efficiency and background suppression are validated through various control channels. There are two Boosted Decision Tree (BDT) involved, the signal region is defined to be the region with $\mathrm{BDT}_1 > 0.9$ and $\eta(\mathrm{BDT}_2) > 0.92$, where the $\eta(\mathrm{BDT}_2)$ is a mapped variable of $\mathrm{BDT}_2$ to make a uniform distribution for signal events. The signal region is further divided into a $4 \times 3$ intervals in the $\eta(\mathrm{BDT}_2) \times q^2_{\mathrm{rec}}$ space, where $q^2_{\mathrm{rec}}$ is the mass squared of the neutrino pair and defined as

$$q^2_{\mathrm{rec}} = s/(4c^4) + M_K^2 - \sqrt{s}E^*_K/c^4,$$

assuming the signal $B$ meson to be at rest in the $e^+e^-$ c.m. frame. Here $M_K$ is the known mass of $K^+$ mesons and $E^*_K$ is the reconstructed energy of the kaon in the c.m. system. For HTA, one BDT is used to suppress the backgrounds and region with $\eta(\mathrm{BDTh}) > 0.4$ is defined as the signal region.

We have conducted dedicated studies to address uncertainties arising from various aspects of the analysis. For instance, on the signal side, we included a dedicated systematic uncertainty for kaon identification and fake rate. The signal selection efficiency was validated using embedded samples, and specific checks were performed for continuum background normalization, $K^0_L$ detection efficiency, and the rescaling of $B \to K^+D(\to K^0_L X)$decays, etc. These efforts ensure a comprehensive assessment of potential uncertainties in the measurement.

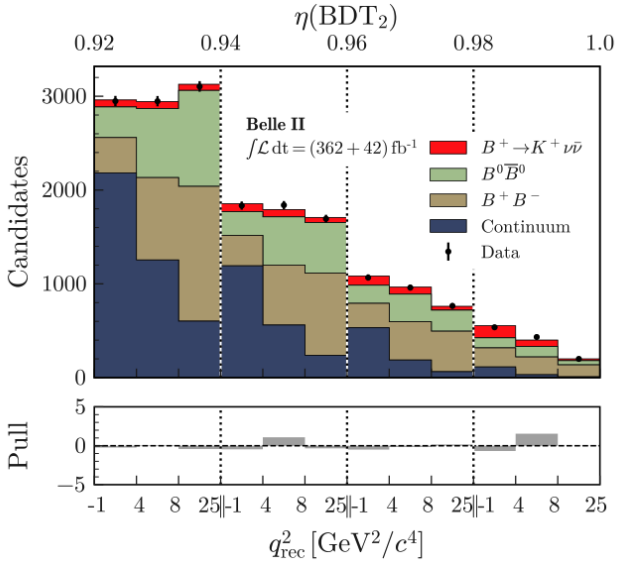


**Figure 10:** Observed yields and fit results in bins of the $\eta(\mathrm{BDT2}) \times q^2_{\mathrm{rec}}$ space obtained by the ITA simultaneous fit to the off- and on- resonance data, corresponding to an integrated luminosity of 42 and 362 $\mathrm{fb}^{-1}$, respectively. The yields are shown individually for the $B^+ \to K^+\nu\bar{\nu}$ signal, neutral and charged $B$-meson decays and the sum of the five continuum categories. The yields are obtained in bins of the $\eta(\mathrm{BDT2}) \times q^2_{\mathrm{rec}}$ space. The pull distributions are shown in the bottom panel.

The signal yields from ITA were extracted by performing a 2-D fit in bins of $[\eta(\mathrm{BDT}_2), q^2_{\mathrm{rec}}]$. The post-fit yields in different signal region with ITA method is shown in Fig. 12, while the post-fit yields from HTA was shown in Fig. 11. The branching fraction obtained from ITA is $\mathcal{B}(B^+ \to$

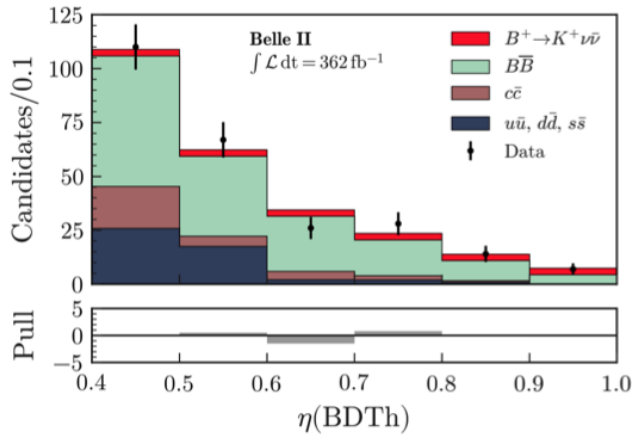


**Figure 11:** Observed yields and fit results in bins of the $\eta$(BDTh) obtained by the HTA method.

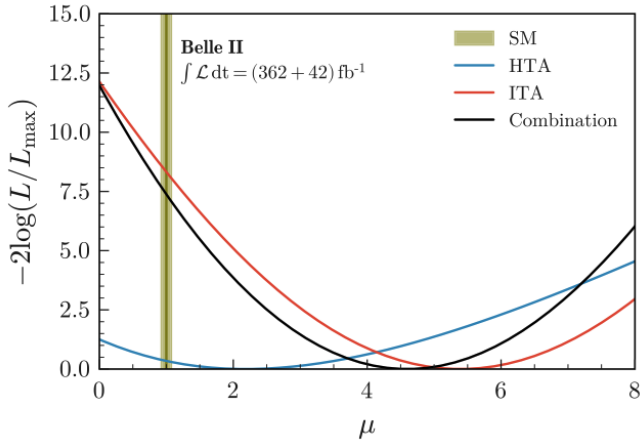


**Figure 12:** The value for each scan point is determined by fitting the data, where all parameters but $\mu$ are varied.

$K^+\nu\bar{\nu}) = (2.7 \pm 0.5 \pm 0.5) \times 10^{-5}$ with a significance of 3.5 standard deviations with respect to the background-only hypothesis, and 2.9 standard deviations with respect to the SM prediction. The branching fraction extracted from HTA is $\mathcal{B}(B^+ \to K^+\nu\bar{\nu}) = (1.1 \pm^{+0.9}_{-0.8} \pm^{+0.8}_{-0.5}) \times 10^{-5}$. The overlap of data sample between ITA and HTA is around 2% of the ITA sample. The results are combined by removing the HTA events from ITA, yielding a branching fraction of $\mathcal{B}(B^+ \to K^+\nu\bar{\nu}) = (2.3 \pm 0.5 \pm^{+0.5}_{-0.4}) \times 10^{-5}$. The combined results has a significance of 3.5 standard deviations with respect to background-only hypothesis and 2.7 relative to SM prediction, providing the first evidence of the $B^+ \to K^+\nu\bar{\nu}$ process [32].

## 5. Study of $\Upsilon(10753)$ at Belle II

The $\Upsilon(10753)$, a bottomonium-like vector state, was observed in the cross-section for the process of $e^+e^- \to \pi^+\pi^-\Upsilon(nS)$ (n=1,2,3) by Belle and in fits to the $e^+e^- \to b\bar{b}$ cross-sections at energies $\sqrt{s}$ from 10.52 to 11.02 GeV. The mass and width of this state are measured to be $M = (10753 \pm 6)$ MeV/c$^2$ and $\Gamma = (36^{+18}_{-12})$ MeV, respectively. Various interpretations have been proposed for this structure, including a conventional bottomonium state, a hybrid, or a tetraquark state, but no definitive explanation has been established so far. Further measurements of the properties and decay modes of the $\Upsilon(10753)$ are crucial for advancing our understanding of its nature and for testing theoretical predictions.

We present an analysis of $\Upsilon(10753) \to \pi^+\pi^-\Upsilon(nS)$ (n=1,2,3) using new, large samples of electron-positron collision data corresponding to 19.6 fb$^{-1}$ collected explicitly for this purpose by the Belle II experiment. We reconstruct decays to $\pi^+\pi^-\Upsilon(nS)$ final states, with the $\Upsilon(nS)$ decaying to a $\mu^+\mu^-$ pair, at $\sqrt{s}$ in the 10.6–10.8 GeV range. We measure and fit the Born cross sections ($\sigma_B$) for these processes as a function of $\sqrt{s}$ to obtain the $\Upsilon(10753)$ mass and width.

We also search for intermediate states to study the internal decay dynamics, such as $e^+e^- \to f_0(980)[\to \pi^+\pi^-]\Upsilon(nS)$ and exotic states like $e^+e^- \to \pi^\pm Z_b(10610, 10650)^\pm[\to \pi^\pm]\Upsilon(nS)$.

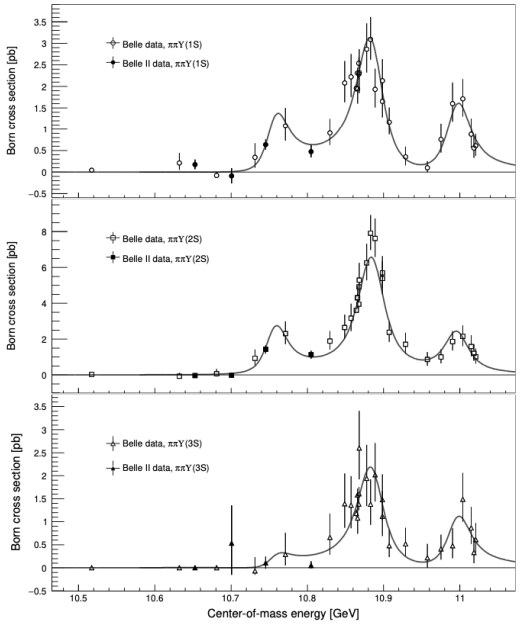


**Figure 13:** Born cross sections for $\pi\pi \to \Upsilon(1S)$(top), $\pi\pi \to \Upsilon(2S)$ (middle), and $\pi\pi \to \Upsilon(3S)$(bottom), with fit results overlaid. Points with error bars show measured cross sections, solid curves are the results of the simultaneous fit results.

The Born cross sections as a function of energy are shown in Fig. 13. The signal for $\pi^+\pi^-\Upsilon(1S)$ and $\pi^+\pi^-\Upsilon(2S)$ are observed with greater than $8\sigma$ significance, while no evidence for $\pi^+\pi^-\Upsilon(3S)$. The observation of $\Upsilon(10753)$ is in agreement with Belle results.

The processes $e^+e^- \to \omega\eta_b(1S)$ and $e^+e^- \to \omega\chi_{b0}(1P)$ are also studied at $\sqrt{s} = 10.745$ GeV. In the tetraquark mode, the decay rate of $\Upsilon(10753) \to \omega\eta_b(1S)$ should be strongly enhanced compared to that of $\Upsilon(10753) \to \pi^+\pi^-\Upsilon(nS)$. Given that the $\eta_b(1S)$ and $\chi_{b0}(1P)$ do not have exclusive decay channels with a large product of efficiency

and branching fraction. Thus the partial reconstruction of an $\omega$ is done in $\pi^+\pi^-\pi^0$ decay and the recoil mass is extracted and used to extract the signal. The fit results of $M_{\text{recoil}}(\pi^+\pi^-\pi^0)$ for the decays $e^+e^- \to \omega\eta_b(1S)$ and $e^+e^- \to \omega\chi_{b0}(1P)$ are shown in Fig. 14. No significant signals are observed, indicating that the tetraquark model are not supported by these results. This study has been summarized in [33].

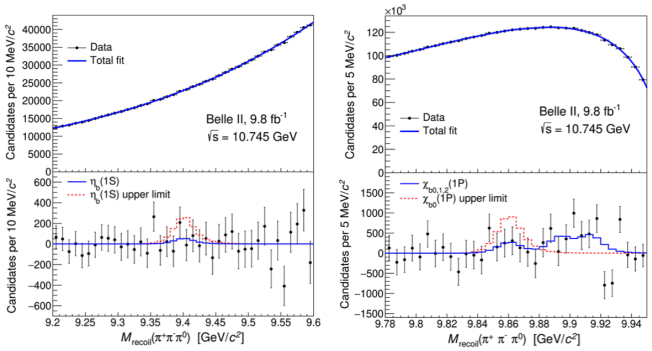


**Figure 14:** Distribution of $M_{recoil}(\pi^+\pi^-\pi^0)$ for the $\pi^+\pi^-\Upsilon(1S)$ (left) and $\pi^+\pi^-\Upsilon(2S)$ (right) candidates. The top distributions show data points with the fit function overlaid, and the bottom shows the data with the background component of the fit function subtracted. The solid histogram shows the fit function for the best fit; the dashed histogram shows the same function with the $J = 0$ yield fixed to the upper limit and $J = 1, 2$ yield set to 0.

## 6. Inputs to the $g_\mu - 2$ anomaly

A discrepancy of approximately five standard deviations has been observed between the world average of the muon anomalous magnetic moment, defined as $a_\mu \equiv (g_\mu - 2)/2$, measured by experiments at BNL [34] and FNAL [35, 36], and SM predictions based on dispersion relations has been reported [37, 38, 39]. The hadronic vacuum polarization (HVP) contribution is the primary source of uncertainty in the SM prediction, accounting for over 80% of the current theoretical uncertainty. Discrepancies between measurements of the cross section have an impact on the uncertainty in the HVP contribution to the $a_\mu$, $a_\mu^{\text{HVP}}$. In the $\pi^+\pi^-$ final state, the long-standing difference from experimental values between BaBar [40] and KLOE [41] contributes to the systematic uncertainty in $a_\mu^{\text{HVP}}$. A recent result from CMD-3 [42, 43] suggests a value closer to the SM prediction. Additionally, recent lattice QCD-based prediction shows a 2-3$\sigma$ difference compared to the values based on dispersion relations, reducing the overall discrepancy to about 1-2$\sigma$. Therefore, it's crucial to perform additional experimental measurements to clarify this situation.

We present a new measurement of the cross section for $e^+e^- \to \pi^+\pi^-\pi^0$ in the energy range from 0.62 to 3.50 GeV using a 191 fb$^{-1}$ data sample from the Belle II experiment and applying an initial-state radiation (ISR) technique [44]. The $e^+e^- \to \pi^+\pi^-\pi^0$ cross section has been measured previously by several $e^+e^-$ experiments. The average uncertainty is quoted as 3% but doesn't include the recent BaBar result [44], which has 1.3% precision. A global fit including the BaBar result achieves a precision of 1.2% [45].

This analysis builds upon the BaBar 2021 measurement in several key aspects. we reconstruct $e^+e^- \to \pi^+\pi^-\pi^0\gamma$ candidates following an initial event selection, extracting the signal by fitting the two-photon mass distribution as a function of $\pi^+\pi^-\pi^0$ mass and determining the yield of $\pi^0 \to \gamma\gamma$ decays. The $3\pi$ mass spectrum is features the $\omega(782)$ and $\phi(1020)$ resonances below 1.05 GeV/c$^2$, the $\omega(1420)$ and $\omega(1650)$ in the range 1.1-1.8 GeV/c$^2$, and $J/\psi$ at 3.09 GeV/c$^2$. Control samples were utilized to estimate the background, which was subsequently subtracted from the observed spectrum. The spectrum was then unfolded to correct for detector resolution effects. The signal efficiency was obtained from simulation and adjusted for discrepancies between data and simulation using various control samples. The key systematic uncertainties include signal selection efficiency and data-MC corrections, with the largest contributions coming from tracking efficiency, ISR photon detection efficiency, $\pi^0$ detection efficiency, and trigger efficiency.

The cross section for this process is given in Fig. 15 compared with previous results.

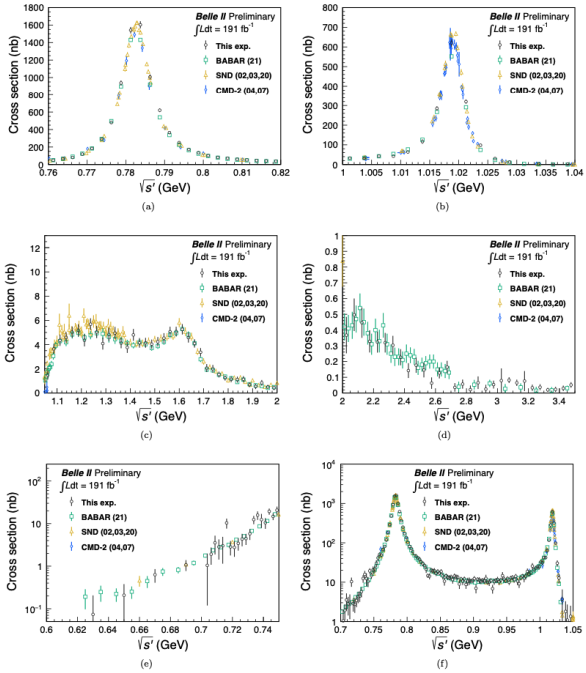


**Figure 15:** Observed $e^+e^- \to \pi^+\pi^-\pi^0$ cross section as a function of energy compared with previous results. Each panel covers a different energy range. Circles with error bars are the Belle II results, squares are the BABAR results, triangles are the SND results, and diamonds are the CMD-2 results.

The systematic uncertainty of the cross section is about 2.2% at the $\omega$ and $\phi$ resonances, where the cross section is relatively large. At other energies, the precision is limited by the statistical uncertainty. The resulting contribution, at

leading order in HVP, to the muon anomalous magnetic moment is $a_\mu^{3\pi} = (48.91 \pm 0.23 \pm 1.07) \times 10^{-10}$ in the $\mu$ 0.62–1.8 GeV energy range. The Belle II result differs by $2.5\sigma$ from the current most precise measurement [44] and global fits [45]. Our next step would be to conduct the measurement in the $\pi^+\pi^-$ final state. This analysis is summarized in [46].

## 7. Conclusion and Prospects

The Belle and Belle II experiments have been and will continue to be able to collect excellent data for various physics programs. We selectively presented some of the recent highlights including the testing of lepton-flavor university by the inclusive test of the $b \to c\tau\nu$ and a light-lepton university tests in $\tau$ decays, measurement of CKM matrix elements, searching for the FCNC transitions in $B$ decays, also the spectroscopy. We also provide inputs to the predicitions of $g_\mu - 2$. We look forward to collect more data in the coming years and push the boundaries of the precise of the measurements.

## References


[1] Latika Aggarwal et al. Snowmass White Paper: Belle II physics reach and plans for the next decade and beyond, 2022.

[2] T. Abe et al. Belle II Technical Design Report. 11 2010.

[3] J. P. Lees et al. Evidence for an Excess of $\overline{B} \to D^{(*)}\tau^-\overline{\nu}_\tau$ Decays. *Phys. Rev. Lett.*, 109:101802, Sep 2012.

[4] J. P. Lees et al. Measurement of an excess of $\overline{B} \to D^{(*)}\tau^-\overline{\nu}_\tau$ decays and implications for charged Higgs bosons. *Phys. Rev. D*, 88:072012, Oct 2013.

[5] M. Huschle et al. Measurement of the branching ratio of $\overline{B} \to D^{(*)}\tau^-\overline{\nu}_\tau$ relative to $\overline{B} \to D^{(*)}\ell^-\overline{\nu}_\ell$ decays with hadronic tagging at Belle. *Phys. Rev. D*, 92:072014, Oct 2015.

[6] I. Adachi et al. A test of lepton flavor universality with a measurement of $R(D^*)$ using hadronic $B$ tagging at the Belle II experiment. 1 2024.

[7] R. Aaij et al. Test of lepton flavor universality using $B^0 \to D^{*-}\tau^+\nu_\tau$ decays with hadronic $\tau$ channels. *Phys. Rev. D*, 108:012018, Jul 2023.

[8] Florian U. Bernlochner, Manuel Franco Sevilla, Dean J. Robinson, and Guy Wormser. Semitauonic $b$-hadron decays: A lepton flavor universality laboratory. *Rev. Mod. Phys.*, 94:015003, Feb 2022.

[9] Keck T. et al. The Full Event Interpretation. *Comput Softw Big Sci*, 2019.

[10] Y. Amhis et al. Averages of $b$-hadron, $c$-hadron, and $\tau$-lepton properties as of 2021. *Phys. Rev. D*, 107:052008, Mar 2023.

[11] I. Adachi et al. First Measurement of $R(X_{\tau/\ell})$ as an Inclusive Test of the $b \to c\tau\nu$ Anomaly. *Phys. Rev. Lett.*, 132:211804, May 2024.

[12] A. Anastassov et al. Experimental tests of lepton universality in $\tau$ decay. *Phys. Rev. D*, 55:2559–2576, Mar 1997.

[13] B. Aubert et al. Measurements of Charged Current Lepton Universality and $|V_{\rm us}|$ Using Tau Lepton Decays to $e^-\overline{\nu}_e\nu_\tau$, $\mu^-\overline{\nu}_\mu\nu_\tau$, $\pi^-\nu_\tau$, and $K^-\nu_\tau$. *Phys. Rev. Lett.*, 105:051602, Jul 2010.

[14] Nicola Cabibbo. Unitary Symmetry and Leptonic Decays. *Phys. Rev. Lett.*, 10:531–533, Jun 1963.

[15] Makoto Kobayashi and Toshihide Maskawa. CP-Violation in the Renormalizable Theory of Weak Interaction. *Progress of Theoretical Physics*, 49(2):652–657, 02 1973.

[16] M. T. Prim et al. Measurement of Angular Coefficients of $\overline{B} \to D^*\ell\overline{\nu}_\ell$: Implications for $|V_{cb}|$ and Tests of Lepton Flavor Universality. *Phys. Rev. Lett.*, 133:131801, Sep 2024.

[17] L. Cao et al. First Simultaneous Determination of Inclusive and Exclusive $|V_{ub}|$. *Phys. Rev. Lett.*, 131:211801, Nov 2023.

[18] M. Hohmann et al. Measurement of the Ratio of Partial Branching Fractions of Inclusive $\overline{B} \to X_u\ell\overline{\nu}$ to $\overline{B} \to X_c\ell\overline{\nu}$ and the Ratio of their Spectra with Hadronic Tagging. 11 2023.

[19] Michael Gronau and David London. Isospin analysis of CP asymmetries in B decays. *Phys. Rev. Lett.*, 65:3381–3384, Dec 1990.

[20] J. Charles et al. Isospin analysis of charmless B-meson decays. *The European Physical Journal C*, Aug 2017.

[21] J. P. Lees et al. Measurement of $CP$ asymmetries and branching fractions in charmless two-body $B$-meson decays to pions and kaons. *Phys. Rev. D*, 87:052009, Mar 2013.

[22] Particle Data Group et al. Review of Particle Physics. *Progress of Theoretical and Experimental Physics*, 2022(8):083C01, 08 2022.

[23] T. Julius et al. Measurement of the branching fraction and $CP$ asymmetry in $B^0 \to \pi^0\pi^0$ decays, and an improved constraint on $\phi_2$. *Phys. Rev. D*, 96:032007, Aug 2017.

[24] F. Abudinén et al. Measurement of the branching fraction and $CP$ asymmetry of $B^0 \to \pi^0\pi^0$ decays using $198 \times 10^6$ $B\overline{B}$ pairs in Belle II data. *Phys. Rev. D*, 107:112009, Jun 2023.

[25] I. Adachi et al. New graph-neural-network flavor tagger for Belle II and measurement of $\sin 2\phi_1$ in $B^0 \to J/\psi K^0_S$ decays. *Phys. Rev. D*, 110:012001, Jul 2024.

[26] P. del Amo Sanchez et al. Search for the decay $B^0 \to \gamma\gamma$. *Phys. Rev. D*, 83:032006, Feb 2011.

[27] I. Adachi et al. Search for the decay $B^0 \to \gamma\gamma$ using Belle and Belle II data. *Phys. Rev. D*, 110:L031106, Aug 2024.

[28] W. G. Parrott, C. Bouchard, and C. T. H. Davies. Standard Model predictions for $B \to K\ell^+\ell^-$, $B \to K\ell^-_1\ell^+_2$ and $B \to K\nu\overline{\nu}$ using form factors from $N_f = 2 + 1 + 1$ lattice QCD. *Phys. Rev. D*, 107:119903, Jun 2023.

[29] T. E. Browder et al. Search for $B \to \tau\nu$ and $B \to K\nu\overline{\nu}$. *Phys. Rev. Lett.*, 86:2950–2954, Apr 2001.

[30] P. del Amo Sanchez et al. Search for the rare decay $B \to K\nu\overline{\nu}$. *Phys. Rev. D*, 82:112002, Dec 2010.

[31] F. Abudinén et al. Search for $B^+ \to K^+\nu\overline{\nu}$ Decays Using an Inclusive Tagging Method at Belle II. *Phys. Rev. Lett.*, 127:181802, Oct 2021.

[32] I. Adachi et al. Evidence for $B^+ \to K^+\nu\overline{\nu}$ decays. *Phys. Rev. D*, 109:112006, Jun 2024.

[33] I. Adachi et al. Search for the $e^+e^- \to \eta_b(1S)\omega$ and $e^+e^- \to \chi_{b0}(1P)\omega$ processes at $\sqrt{s} = 10.745$ GeV. *Phys. Rev. D*, 109:072013, Apr 2024.

[34] G. W. Bennett et al. Final report of the E821 muon anomalous magnetic moment measurement at BNL. *Phys. Rev. D*, 73:072003, Apr 2006.

[35] B. Abi et al. Measurement of the Positive Muon Anomalous Magnetic Moment to 0.46 ppm. *Phys. Rev. Lett.*, 126:141801, Apr 2021.

[36] D. P. Aguillard et al. Measurement of the Positive Muon Anomalous Magnetic Moment to 0.20 ppm. *Phys. Rev. Lett.*, 131:161802, Oct 2023.

[37] T. Aoyama et al. The anomalous magnetic moment of the muon in the Standard Model. *Physics Reports*, 887:1–166, 2020. The anomalous magnetic moment of the muon in the Standard Model.

[38] Alexander Keshavarzi, Daisuke Nomura, and Thomas Teubner. Muon $g - 2$ and $\alpha(M_Z^2)$: A new data-based analysis. *Phys. Rev. D*, 97:114025, Jun 2018.

[39] M. Davier et al. A new evaluation of the hadronic vacuum polarisation contributions to the muon anomalous magnetic moment and to $\alpha(m_Z^2)$. *The European Physical Journal C*, 2020.

[40] J. P. Lees et al. Precise measurement of the $e^+e^- \to \pi^+\pi^-(\gamma)$ cross section with the initial-state radiation method at BABAR. *Phys. Rev. D*, 86:032013, Aug 2012.

[41] A. Anastasi et al. Combination of KLOE $\sigma(e^+e \to \pi^+\pi^-\gamma(\gamma))$ measurements and determination of $a_\mu^{\pi^+\pi^-}$ in the energy range $0.10 < s < 0.95$ GeV$^2$, journal = Journal of High Energy Physics. 2018.

[42] F. V. Ignatov et al. Measurement of the $e^+e^- \to \pi^+\pi^-$ cross section from threshold to 1.2 GeV with the CMD-3 detector. *Phys. Rev. D*, 109:112002, Jun 2024.

[43] F. V. Ignatov et al. Measurement of the Pion Form Factor with CMD-3 Detector and Its Implication to the Hadronic Contribution to Muon

$(g-2)$. *Phys. Rev. Lett.*, 132:231903, Jun 2024.
[44] J. P. Lees et al. Study of the process $e^+e^- \to \pi^+\pi^-\pi^0$ using initial state radiation with BABAR. *Phys. Rev. D*, 104:112003, Dec 2021.
[45] Martin Hoferichter et al. Isospin-breaking effects in the three-pion contribution to hadronic vacuum polarization. *Journal of High Energy Physics*, 2023:208, 2023.
[46] I. Adachi et al. Measurement of the $e^+e^- \to \pi^+\pi^-\pi^0$ cross section in the energy range 0.62-3.50 GeV at Belle II, 2024.